ARTICLES

Measurement of the $\pi^+ \to e^+\nu$ branching ratio

D. I. Britton,* S. Ahmad,† D. A. Bryman, R. A. Burnham,‡ E. T. H. Clifford,§
P. Kitching, Y. Kuno,‖ J. A. Macdonald, T. Numao, A. Olin, and
J-M. Poutissou
TRIUMF, Vancouver, British Columbia, Canada V6T 2A3

M. S. Dixit
Centre for Research in Particle Physics, Carleton University, Ottawa, Ontario, Canada K1S 5B6
(Received 4 June 1993)

A measurement of the $\pi^+ \to e^+\nu$ branching ratio gives $R_{\pi e\nu} = \Gamma(\pi \to e\nu + \pi \to e\nu\gamma)/\Gamma(\pi \to \mu\nu + \pi \to \mu\nu\gamma) = 1.2265 \pm 0.0034(\text{stat}) \pm 0.0044(\text{sys}) \times 10^{-4}$. This result is in agreement with standard model calculations and confirms the hypothesis of electron-muon universality at the 0.2% level.

PACS number(s): 13.20.Cz, 11.30.Hv, 14.40.Aq, 14.60.−z

I. INTRODUCTION

The helicity-suppressed decay $\pi^+ \to e^+\nu$ was first discovered in 1958 [1] and provided a confirmation of the $V - A$ theory [2] of weak interactions. Because it is one of the exceptional weak processes that is both calculable and measurable to high precision and provides a test of the universal coupling scheme for the electron and the muon, the decay $\pi^+ \to e^+\nu$ has been important in the development of weak interaction theory and the standard model. The concept of lepton universality in the context of the three known generations can now be tested at different mass scales with π, τ, and W leptonic decays. Marciano [3] has emphasized that the branching ratio of the decays $\pi^+ \to e^+\nu$ and $\pi^+ \to \mu^+\nu$ tests charged-current μ-e universality in the longitudinal component of the W coupling, whereas τ and W decays test the transverse component. Measurement of the $\pi^+ \to e^+\nu$ branching ratio provides the most stringent test of lepton universality.

Extensions of the standard model [4] leading to a deviation from the universal gauge coupling scheme could involve massive neutrinos and nonzero off-diagonal matrix elements connecting weak and mass eigenstates of neutrinos [5]. Models predicting massive neutrinos, such as mirror neutrinos [6] or fourth-generation neutrinos, generally exhibit "violation" of lepton universality. The introduction of new gauge bosons for each generation was discussed by Li and Ma [7], and a similar approach was taken by Fayyazuddin and Riazuddin [8] who proposed individual U(1) symmetries for each generation. The existence of hypothetical particles such as Majorons [9] or charged Higgs scalars arising from extended symmetries [10, 11] could also influence the $\pi^+ \to e^+\nu$ branching ratio. Because the $\pi^+ \to e^+\nu$ decay is helicity suppressed, it is sensitive to the presence of pseudoscalar couplings. A pseudoscalar interaction could interfere with the dominant axial-vector component, and the deviation from the standard model prediction is proportional to $1/m_H^2$, where m_H is the mass of the exotic particle that carries the pseudoscalar interaction. This is in contrast to hypothetical lepton flavor-violating processes where the calculated rate is usually proportional to $1/m_H^4$. Precise measurements of the decay $\pi^+ \to e^+\nu$ therefore provide critical tests of the foundation of the standard model and its possible extensions.

The observed branching ratio $R_{\text{expt}} = \frac{\Gamma(\pi \to e\nu + \pi \to e\nu\gamma)}{\Gamma(\pi \to \mu\nu + \pi \to \mu\nu\gamma)}$ involves the effect of physical and virtual photons. Without radiative corrections, the $\pi^+ \to e^+\nu$ branching ratio would be $R_{\text{th}} = 1.284 \times 10^{-4}$; the suppression is the result of a helicity factor $(m_e/m_\mu)^2$ arising from the $V - A$ nature of the interaction. Early calculations by Berman [12] and Kinoshita [13] for the radiative corrections assuming a pointlike pion showed that the infrared divergences in virtual-photon and inner-bremsstrahlung corrections canceled in the total rate and the largest correction was of the order of $\delta = (3\alpha/\pi)\ln(m_e/m_\mu)$. Using an ultraviolet cutoff for the virtual-photon energy chosen arbitrarily to be the same for the e and μ cases, the calculated $\pi^+ \to e^+\nu$ branching ratio was $R_{\text{th}} = 1.233 \times 10^{-4}$.

It was shown by Goldman and Wilson [14] that the question of cutoffs could be treated unambiguously in a gauge model with a point-pion field. In a subsequent definitive calculation, Marciano and Sirlin [15] demon-

*Present address: McGill University, Montreal, Quebec, Canada H3A 2T8.
†Present address: Rice University, Houston, Texas 77251.
‡Deceased.
§Present address: P.O. Box 611, Deep River, Ontario, Canada K0J 1P0.
‖Present address: KEK, Tsukuba-shi, Ibaraki-ken, Japan 305.

strated that the presence of strong interactions (pion structure) does not affect the cancellation of the divergence and the correction δ is essentially fixed by gauge invariance. They also showed that interference terms between the structure-dependent and non–structure-dependent diagrams cancel in first order. At this point, the only uncalculable (or model-dependent) first-order approximation was a pure structure-dependent inner-bremsstrahlung term which was phenomenologically parametrized using vector (F_V) and axial-vector (F_A) coupling constants [15, 16]. In this approach, F_V was estimated from the lifetime of the π^0 based on the conserved vector current theory, and the measurements of the $\pi^+ \to e^+\nu\gamma$ [17] and $\pi^+ \to e^+\nu e^+e^-$ [18] decays determined the axial-vector constant $F_A \simeq 0.5F_V$. This resulted in a very small structure-dependent contribution for the $\pi^+ \to e^+\nu$ branching ratio. Terent'ev came to the same conclusion based on the partially conserved axial-vector current hypothesis [19]. The resulting $\pi^+ \to e^+\nu$ branching ratio with radiative corrections expected in the standard model assuming universality [3] is

$$R_{\rm th} = \frac{\Gamma_{\rm th}(\pi \to e\nu + \pi \to e\nu\gamma)}{\Gamma_{\rm th}(\pi \to \mu\nu + \pi \to \mu\nu\gamma)} = (1.2350 \pm 0.0005) \times 10^{-4}, \quad (1)$$

where the uncertainty arises from presently uncalculated structure-dependent loop effects.

The first precise measurement of the $\pi^+ \to e^+\nu$ branching ratio $R_{\rm expt}$ was done by Anderson *et al.* [20] using a magnetic spectrometer. They measured positrons from the decay $\pi^+ \to e^+\nu$ ($E_{e^+} = 69.3$ MeV) and from the decay $\pi^+ \to \mu^+\nu$ followed by the decay $\mu^+ \to e^+\nu\bar{\nu}$ (the $\pi^+ \to \mu^+ \to e^+$ chain decay, $E_{e^+} = 0$–52.3 MeV). After adding inner radiative corrections of 2.5%, the measured branching ratio was $R_{\rm expt} = (1.21 \pm 0.07) \times 10^{-4}$. Another experiment, by Di Capua *et al.* [21], used a 23-cm-diam × 24-cm-long NaI detector that is sensitive to both photons and charged particles. The measurement, therefore, included most of the inner-bremsstrahlung effect. They invented a "bin method" in which the $\pi^+ \to e^+\nu$ and $\pi^+ \to \mu^+ \to e^+$ decays were detected during two equal time bins separated by several pion lifetimes. $R_{\rm expt}$ deduced in this method avoids several potential systematic errors such as the muon contamination in the beam, the time bin width, and the detector solid angle. From the sample of 10^4 $\pi^+ \to e^+\nu$ events they obtained $R_{\rm expt} = (1.247 \pm 0.028) \times 10^{-4}$; this result was subsequently revised to $R_{\rm expt} = (1.273 \pm 0.028) \times 10^{-4}$ to account for a change in the experimental pion lifetime [22].

Using a similar technique but with a NaI detector 8 times larger in volume and 2 times better in energy resolution [5.5% full width at half maximum (FWHM) at the $\pi \to e\nu$ peak], along with a detailed timing analysis to separate $\pi^+ \to e^+\nu$ and $\pi^+ \to \mu^+ \to e^+$ decays, Bryman *et al.* [23] found $R_{\rm expt} = (1.218 \pm 0.014) \times 10^{-4}$ from a sample of 3×10^4 $\pi \to e\nu$ events. The largest systematic uncertainty (0.75%) came from limited knowledge of the NaI response spectrum; the low-energy tail associated with the $\pi^+ \to e^+\nu$ peak extended into the energy region of the distribution from the $\pi^+ \to \mu^+ \to e^+$ decay chain. Two new results have been reported recently [24, 25]. This paper is a detailed description of the TRIUMF experiment [24].

II. EXPERIMENT

The branching ratio $R_{\rm expt}$ can be obtained from the ratio of positron yield from the $\pi^+ \to e^+\nu$ decay ($E_{e^+} = 69.3$ MeV) to that from the $\pi^+ \to \mu^+ \to e^+$ chain decay ($E_{e^+} = 0$–52.3 MeV). By not relying on direct detection of the decay $\pi^+ \to \mu^+\nu$, many normalization factors, such as the solid angle of positron detection and the number of incident pion stops, cancel in first order, and only small energy-dependent effects like those due to multiple Coulomb scattering and positron annihilation need to be corrected for. The positron spectrum is divided into low-energy ($\pi \to \mu \to e$) and high-energy ($\pi \to e\nu$) regions at the end point of the $\pi^+ \to \mu^+ \to e^+$ decay. Simultaneous fitting of the time distributions of low- and high-energy regions provides the yields of $\pi^+ \to \mu^+ \to e^+$ decay and $\pi^+ \to e^+\nu$ decay, respectively. One of the major uncertainties of the previous experiments was due to the low-energy tail of $\pi^+ \to e^+\nu$ events that was buried under the large $\pi^+ \to \mu^+ \to e^+$ population. In the present experiment, the $\pi^+ \to e^+\nu$ decay was enhanced using a technique which suppressed events with additional energy in the stopping counter due to $\pi \to \mu$ decay so that an empirical measurement of the tail could be made.

A. Experimental setup

The experiment [24] was carried out using a π^+ beam of momentum 83 ± 1 MeV/c on the low-energy pion channel $M13$ which viewed a 10-mm-thick graphite production target in a 500-MeV, 100-μA proton beam from the TRIUMF cyclotron. The setup is shown schematically in Fig. 1. The incoming beam consisting of 80% pions, 10% muons, and 10% positrons had a microstructure corresponding to the 23-MHz cyclotron radio frequency (rf), and each type of particle had a characteristic time of flight (TOF) from the production target with respect to the rf. The beam was detected in a plastic scintillation counter $B1$ (76 mm × 76 mm × 13 mm) and defined transversely by L-shaped veto counters VL and VR arranged to form a 25-mm × 25-mm aperture. Pions were stopped in the target counter assembly which consisted of the plastic scintillator $B3$ (76 mm × 76 mm × 13 mm) as the central element enclosed by 1.6-mm-thick $B2$, $B4$, LL, and LR counters. The whole assembly was tilted by 45° to the beam direction. Pions at a rate of 10^5 s^{-1} were brought to the target and 70% of them stopped in the fiducial region at a depth of 5 mm from the downstream side of $B3$ with a distribution width of 5 mm (FWHM). Beam particles which penetrated the target assembly were detected by the $V0$ counter. The muons from $\pi^+ \to \mu^+\nu$ decays of stopped pions have a range of 1.5 mm in a plastic scintillator and were fully confined within the target counter array.

Positrons from the decays of stopped pions in the tar-

get were detected at 90° to the beam, passing through the $B4$ counter, two planar 203-mm × 203-mm proportional wire chambers for position measurement, and a telescope of three 1.6-mm-thick plastic scintillation counters $T1$–3 and a 3.2-mm-thick counter $T4$. The positron energy was analyzed in a 460-mm-diam × 510-mm-long NaI(Tl) crystal "TINA." The solid-angle acceptance of 2.9% was determined by the 152-mm-diam counter $T4$. The counters $T2$ and $T3$ entirely covered the front face of TINA and served to detect additional charged particles entering TINA.

There was a muon halo in the beam originating from pion decays in flight, and some muons could hit the T counters, simulating decay positrons. In order to tag those events, a 400-mm-long, 200-mm-wide plastic counter $V1$ with a 90° bend in the middle was placed at the upstream side of the T counters as shown in Fig. 1.

Timing of the incoming pion was obtained from $B2$ and timing of the positron event from $T4$. The event time relative to the stopping pion was measured with a time-to-amplitude converter (TAC, ORTEC 467) feeding an analog-to-digital converter (ADC, LeCroy 3512) to optimize linearity. The other signal times were measured using time-to-digital converters (TDC, LeCroy 2228 series) either with respect to the arrival time of a pion for beam-related signals or to a positron event time for event-related signals. Pulse heights from most scintillation counters were recorded by two ADC's (LeCroy 2249 series) with 30-ns- and 200-ns-wide gates; this enabled pileup detection resolution as close as 10 ns. The ADC gates were derived from $B2$ or $T4$ depending on the source of the signal. In order to record more detailed pulse shape information from $B3$, a linear-gate module (Phillips 744) located close to the scintillator was used

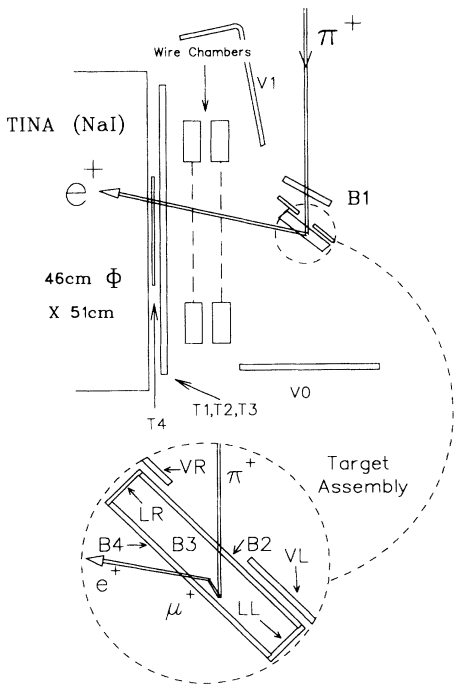

FIG. 1. Schematic view of the experimental setup. Details of the target assembly are shown in the inset.

to sample the leading 3, 5, and 7 ns of the signal. These three outputs were digitized by ADC's with a standard 30-ns-wide gate. The fourth ADC had a 200-ns-wide gate which covered the entire decay sequence, and the fifth was gated at the time of the positron event. The combined signal from TINA was shaped with a time constant of 0.5 μs using a linear amplifier (TENNELEC TC205A) in order to get good energy resolution, and the pulse height was measured with an ADC (LeCroy 3512) in a peak-sensing mode. The gain matching of the seven photomultipliers (RCA 4522) which viewed the NaI crystal was monitored using the high-energy edge of the $\mu^+ \rightarrow e^+\nu\bar{\nu}$ decay spectrum, and adjusted daily by resetting the high voltages.

To detect beam pileup [23], the logical OR of the signals from the counters $B1$, VL, and VR was examined for 6 μs before and after a valid pion stop, and the closest arrival time of any additional beam particle was recorded with TDC's. The signals from the counters $B1$, $B2$, VL, VR, LL, and LR were digitized using ADC's with a 200-ns-wide gate centered on the main pulse, and the pulse height information provided additional protection against a pileup close to the pion stop. A similar technique was used to measure charged-particle pileup in TINA; the logical OR of the signals from the counters $T1$, $T2$, and $T3$ was examined for 6 μs before and after the event, and the signal from $T3$ was also recorded with an ADC with a 200-ns-wide gate.

The trigger was arranged in two levels. The first level was based on a delayed coincidence, between the beam defined by $B1 \cdot B2 \cdot (\overline{V0 + VL + VR})$ and the decay positron defined by $T4 \cdot (T1 + T2 + T3)$, within the time range $-120 < t_0 < 300$ ns with respect to the pion stop time t_0. This initiated gate signals to the ADC's and TDC's. The second level trigger was designed to favor $\pi \rightarrow e\nu$ events and consisted of all events occurring within 30 ns after a pion stop (BIN1), or having a deposited energy above ~45 MeV (corresponding to an initial positron energy of ~50 MeV) in TINA (TINA45). An unbiased sample of $\pi \rightarrow \mu \rightarrow e$ and background events was taken by another second-level trigger source formed from (1:16)-prescaled first-level triggers (UNBIAS). A reset signal was generated if the event did not satisfy any second-level trigger requirement. The trigger pattern was recorded with each event.

Typical event rates were 25, 15, and 5 s^{-1} for the BIN1, UNBIAS, and TINA45 triggers, respectively. The event size was 75 16-bit words. Data were taken over a period of 3 months in 1986, and roughly 8×10^7 BIN1 events, 5×10^7 UNBIAS events, and 10^7 TINA45 events (containing 4×10^5 $\pi \rightarrow e\nu$ decay events) were written onto tape through a CAMAC–PDP-11/34 data acquisition system.

B. Other data

Various sets of test and calibration data were taken with modified trigger conditions. For example, to study the effect of vetoing by the $V0$, VL, and VR counters, some runs were taken without requiring any conditions in those counters. Large acceptance runs were taken by replacing the role of the solid-angle defining counter $T4$

by a coincidence of $T2$ and $T3$. The beam rate was also varied between 5×10^4 and 2×10^5 s^{-1}.

The position of the prompt time t_0 in the TAC spectrum was measured using the standard data acquisition configuration but the beam momentum was scaled so that beam muons stopped in the target counter $B3$ at the same depth. The data acquired in this mode consisted of $\mu^+ \to e^+\nu\bar{\nu}$ events which had a time distribution decaying with the muon lifetime from a maximum at t_0. The shape of the time distribution edge at t_0 also gave the time resolution of the system as a function of the energy deposited in TINA.

The linearity of the timing electronics was measured by generating random starts with a radioactive source adjacent to the counter $T4$ to simulate events during beam-off periods. This information was used to correct the timing spectrum. The TDC and TAC-ADC time calibration was obtained using a signal derived from the cyclotron rf.

Response functions of TINA were measured using a low-rate positron beam (100–1000 s^{-1}). The crystal was positioned in the beam and data were taken with the crystal axis at 0°, 10°, and 20° to the beam axis to simulate the various trajectories of the positrons entering the crystal in the experiment. This was repeated at five positron energies between 20 and 85 MeV.

III. ANALYSIS

The positron energy spectrum is shown in Fig. 2 and timing spectra for the high-energy ($\pi \to e\nu$) and low-energy ($\pi \to \mu \to e$) regions are given in Figs. 3(a) and 3(b), respectively. These spectra were obtained by applying cuts (Sec. III A) designed to eliminate background events without causing dependence on the positron energy. The timing spectra were fitted to obtain a raw branching ratio. Fitting the timing spectra, instead of taking a ratio of numbers of events, has all the virtues of the "bin method" mentioned above. It also allows for tests of other systematic effects by facilitating inclusion of possible distortions.

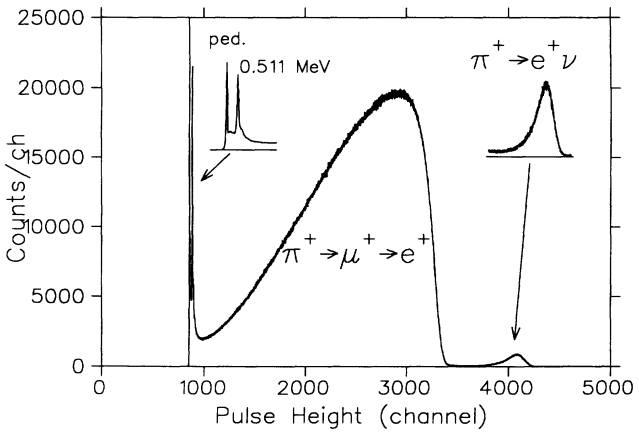

FIG. 2. Positron energy spectrum for early time (< 30 ns). The two peaks at low energy (shown in the inset) are due to the zero-energy pedestal and the 0.511-MeV annihilation γ rays from low-energy positrons which satisfy the trigger requirement but do not penetrate TINA. The two peaks account for 0.7% of the $\pi \to \mu \to e$ counts.

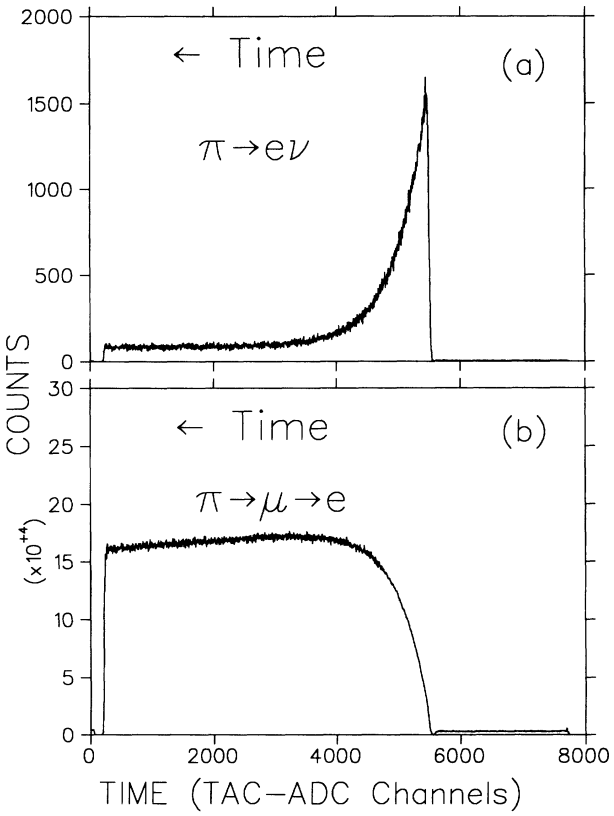

FIG. 3. Time spectra for (a) the upper ($\pi \to e\nu$) and (b) lower ($\pi \to \mu \to e$) parts of the energy spectrum divided at channel 3400 in Fig. 2.

A. Gain correction and calibration

Discrete timing shifts in the TDC spectra, due mostly to changes of electronics modules, were corrected on a run-by-run basis. In addition to the usual long-term gain drifts, there were also rapid gain changes in ADC data over a period of minutes after sudden beam rate changes. These were corrected on an event-by-event basis based on a running average of the peak position in each spectrum. The gain was adjusted according to the difference between the expected and actual peak positions. The number of events chosen to determine the average was typically 1000–6000 events, corresponding to a data-taking period of 10–100 s. For the stabilization of TINA, the upper edge of the $\mu^+ \to e^+\nu\bar{\nu}$ decay spectrum was used.

The positron energy calibration was established by using the peak due to the $\pi^+ \to e^+\nu$ decay and the edge of the $\pi^+ \to \mu^+ \to e^+$ decay distribution, together with the pedestal peak of 4.9 MeV corresponding to the estimated energy loss in the beam and telescope counters and the entrance window of TINA. The positron energies quoted throughout this paper are initial kinetic energies unless otherwise noted.

B. Event selection

A pion stop in the target counter $B3$ was defined by a prompt coincidence $B1 \cdot B2 \cdot B3 \cdot (\overline{B4 + V0 + VL + VR})$. TOF (with respect to the cyclotron rf signal) and energy loss in the beam counters were used to select pions and reject muons and positrons in the beam (see Fig. 4). The energy-loss cut criteria defined a single-pion window that removed events with an extra beam particle in the same rf burst and events triggered by a false beam signal due to a decay positron. Inclusion of the $B4$ counter as a veto in the beam logic rejected a few good events in which a pion stopped in $B3$ and the decay muon went into $B4$ within 3 ns after a pion stop. However, the lost component, in which the pion had become a muon before event inspection, could be treated as a part of the beam muon term in the timing spectrum discussed below. It was shown that the lost component had no effect on the branching ratio (see Sec. III C). An early decay positron also caused a false $B4$ veto count and was rejected. However, as long as the early time region was excluded from the analysis this did not affect the branching ratio.

The event definition in the off-line analysis was a coincidence of the signals in all the T counters and the $B4$ counter as well as hits in the two wire chambers. Because a signal from TINA was not required in the event definition, there were a few low-energy events in which the positron stopped in the last trigger counter $T4$ or the entrance window of TINA. These positrons produced two collinear 0.511-MeV annihilation γ rays, only one of which could enter TINA. If both γ rays missed TINA, the events contributed to the zero-energy pedestal peak. The two peaks at 0 and 0.511 MeV are evident in Fig. 2.

Prompt protons extending to ~110 MeV were produced by beam pions via (π^+, p) reactions in the target region. They were easily distinguished from the minimum-ionizing positrons by their high energy loss in $T1$–4. The information from the four scintillators was combined to produce a nearly Gaussian energy-loss distribution by choosing the minimum of the three calibrated pulse heights from $T1$, a sum of $T2$ and $T3$, and $T4$ (Fig. 5). The cut to reject protons was applied to the energy-loss spectrum as a function of energy deposited in TINA (the heavy line in Fig. 5). The events removed were examined for a possible energy-dependent effect, and it was concluded that the bias in the final branching ratio was $\leq 0.04\%$. Although the above cut did not remove pions that scattered elastically or inelastically to the telescope counters, they were relatively few and the effect was found to be negligible. A lower cut on the energy loss was applied to eliminate events in which a positron hit the light guide of the $T4$ counter producing Čerenkov light. Good events were not removed by this cut.

If additional particles entered TINA before or after the event, the energy resolution was degraded due to pulse pileup; positrons from the $\mu^+ \rightarrow e^+ \nu \bar{\nu}$ decay were shifted to higher energy as shown in Fig. 6, where the time of post pileup versus the energy deposited in TINA is plotted. This caused background in the time spectrum of high-energy events (the $\pi \rightarrow e\nu$ region). These effects were minimized by removing pileup events between 0 and ± 1.2 μs as shown by the vertical line in Fig. 6. Within

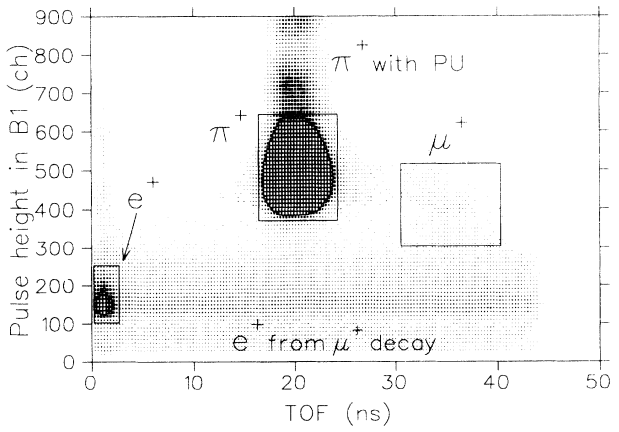

FIG. 4. TOF vs pulse heights in the $B1$ counter. Boxes indicate beam particles. Some counts above the boxes are due to an additional particle in the same ADC gate (indicated by PU). The density scale is nonlinear in order to enhance rare events.

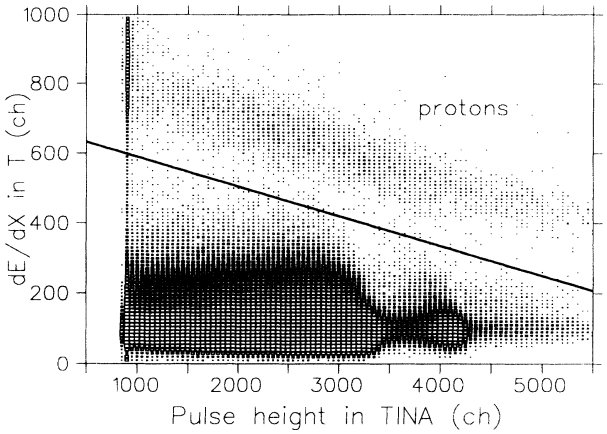

FIG. 5. TINA energy vs energy loss in the T counters. The heavy line indicates the cut position used to eliminate protons. The density scale is nonlinear.

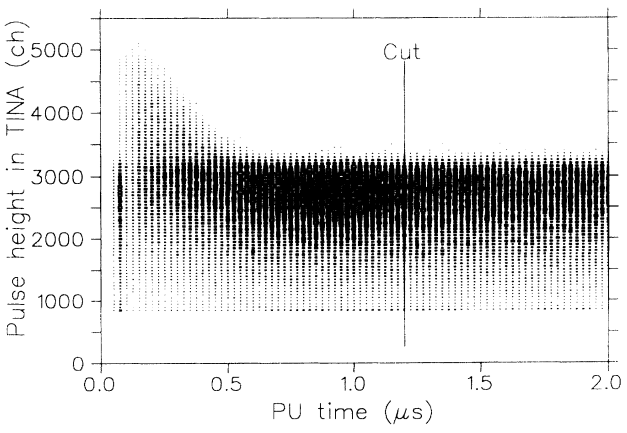

FIG. 6. Time of postpileup vs TINA energy. The vertical line indicates the cutoff time at 1.2 μs which rejected ~3% of good events.

the resolving time of the pileup detection system, a comparison between ADC's with a 30-ns-wide gate (mostly sensitive to the main pulse) and a 200-ns-wide gate (sensitive to a pileup as well as the main pulse) provided additional pileup information (see Sec. IV B for a similar technique). The cut removed only 0.05% of single-track events with negligible energy dependence.

The branching ratio measurement could potentially be affected by distortions in positron decay time or energy measurements due to the presence of extra beam pions in the event time window, and events with an additional beam particle between 20 and 370 ns with respect to a pion stop were rejected by a postpileup cut. The time region within ± 100 ns of the pion stop was, as mentioned earlier (Sec. II A), covered by wide-gate ADC's on $B1$, VL, and VR. Because the muon lifetime is long, additional pions arriving prior to the valid stop increase the background with the muon lifetime in the entire time spectrum. There was also a distortion around 30 ns before the time zero in the time spectrum of the high-energy region ($\pi \to e\nu$) as discussed in Sec. III C. The effect was enhanced when multihit events in the wire chambers were selected; this feature was a result of charged-particle pileup in TINA caused by inefficiency in the pileup logic around the time of the event due to a finite pulse width. The distortion in the high-energy time spectrum was reduced by an order of magnitude to a negligible level (less than 0.05% of the $\pi \to e\nu$ events) by employing a tight prepileup cut extending to -5 μs; this also resulted in a significant reduction of the background with the muon lifetime.

Wire-chamber data were used to eliminate positrons originating outside the target and those which scattered in the wire-chamber frames. The cut, corresponding to the geometrical acceptance of the $T4$ counter (9.6 cm in diameter at the front wire-chamber position), rejected 1.4% of events. There was potentially a strong dependence (see Sec. IV A) of the measured branching ratios on this diameter cut as shown by solid circles in Fig. 7. Multiple-track events were retained in the analysis in order to avoid vetoing events with positrons back scattered from the T counters and TINA. This effect will be discussed in Sec. IV C.

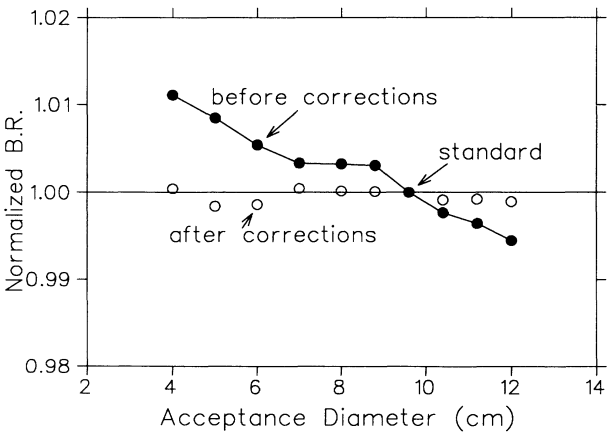

FIG. 7. Effects of positron trajectory cuts based on a circle of acceptance defined by the wire chambers. The solid (open) circles indicate normalized branching ratios to the standard value at 9.6 cm before (after) the Monte Carlo and tail corrections.

Events with a signal in $V1$ at the time of event were rejected in the analysis, thus minimizing triggers due to beam muons directly hitting the T counters. The majority of muon-initiated events were also removed by the coincidence requirement of $B4$ in the event definition and by the fiducial cuts based on wire-chamber information.

Figure 2 shows the energy spectrum of selected positron events in the time region 5–30 ns, consisting of a peak at 69.3 MeV with $\sim 1.2 \times 10^5$ $\pi \to e\nu$ decay events and a distribution from the $\pi \to \mu \to e$ decay events.

C. Timing fit

A raw branching ratio R' was determined by simultaneous fitting of the measured positron decay-time spectra shown in Figs. 3(a) and 3(b). These are the distributions for events above and below an energy threshold at 56.4 MeV (channel 3400) in the TINA energy spectrum, corresponding to $\pi^+ \to e^+\nu$ and $\pi^+ \to \mu^+ \to e^+$ decays, respectively.

Some distortions due to nonlinearities in the TAC-ADC system were first removed by rebinning the time spectra. The Fourier frequencies obtained from the oscillation pattern in the linearity-test spectra were stable and had two main components; one corresponded to the clock frequency of the ADC ($\sim$300 MHz) and the others corresponded to some multiple of 1/512 ch^{-1}. Because the oscillation amplitude for each frequency varied from time to time, it was not used directly in the correction. The deviations of a high-statistics $\pi \to \mu \to e$ time spectrum with minimal cuts from the expected time distribution were used to extract the amplitudes and phases of those oscillation components for actual data. The rebinning widths were obtained from the resultant amplitude and phase of each frequency.

The timing fit was done using the program MINUIT [26]. The equation for the high-energy ($\pi \to e\nu$) region is

$$F_{\pi e\nu}(t) = A_\pi \left[R'\lambda_\pi e^{-\lambda_\pi t} + \xi_{\pi\mu e} f(t)\right] \theta(t) + A_{\mathrm{BG1}} e^{-\lambda_\mu t} + C_{\mathrm{BG1}}, \quad (2)$$

where the time spectrum for the decay $\pi \to \mu \to e$ is given by $f(t) = \frac{\lambda_\pi \lambda_\mu}{\lambda_\pi - \lambda_\mu}(e^{-\lambda_\mu t} - e^{-\lambda_\pi t})$, $t = t' - t_0$ for measured time t' and pion stop time t_0, and $\theta(t) = 0$ for $t < 0$ and $\theta(t) = 1$ for $t > 0$. A_π, R', $\xi_{\pi\mu e}$, A_{BG1}, and C_{BG1} are the total number of genuine events, the raw $\pi \to e\nu$ branching ratio, the fraction of $\pi \to \mu \to e$ events above the cutoff energy (due mostly to pileup), a background amplitude with the muon lifetime (due to "old" muons in the target), and a constant background, respectively; $\lambda_\pi = (26.03\ \mathrm{ns})^{-1}$ and $\lambda_\mu = (2197.03\ \mu\mathrm{s})^{-1}$ are the pion and muon decay rates [22]. A Gaussian function was folded into the above equation to include timing resolution effects. (The branching ratio was found to be insensitive to the timing resolution which was measured to be 0.57 ± 0.02 ns.) The time spectrum for the low-

energy ($\pi \to \mu \to e$) region is

$$F_{\pi\mu e}(t) = A_\pi \left[(1 - \xi_{\pi\mu e}) f(t)\right] \theta(t) + A_{\mathrm{BG2}} e^{-\lambda_\mu t} + C_{\mathrm{BG2}}, \quad (3)$$

where A_{BG2} and C_{BG2} are a background amplitude with the muon lifetime and a constant background, respectively. The constant background terms in Eqs. (2) and (3) were used to approximate the component from a slowly decaying background (e.g., due to inefficiency in the beam pileup logic) if C_{BG} is positive, or from a short-lifetime background if C_{BG} is negative. The fitting ranges were −100 to −6.5 ns and 5.5 to 240 ns for both spectra, chosen to avoid the lowest and highest channel regions which had large nonlinearities, and also the t_0 region which was vulnerable to potential distortion from prompt π-nuclear reaction products. A_π, R', $\xi_{\pi\mu e}$, t_0, and all background amplitudes were free parameters in the fit. The above equations do not explicitly have a component describing stopped muons with a time dependence $e^{-\lambda_\mu t}$ starting at t_0. Inclusion of such a term is mathematically identical to changing t_0. This term was therefore omitted and the time zero parameter t_0 was set free in the fit. It should be noted that the branching ratio is essentially determined by the ratio of the amplitudes of the terms with $e^{-\lambda_\pi t}$ in Eq. (2) and in Eq. (3) as a part of $f(t)$, i.e., of the terms describing $\pi^+ \to e^+\nu$ and $\pi^+ \to \mu^+\nu$ decays, respectively. Early pion decays into $B4$ which have been rejected by the stop definition do not contribute to the amplitude of the $e^{-\lambda_\pi t}$ term and therefore have no effect on the branching ratio.

The combined fit gave $R' = 1.1994 \pm 0.0034(\mathrm{stat}) \pm 0.0023(\mathrm{sys}) \times 10^{-4}$ with a χ^2 per degree of freedom of 1.47. The statistical error was obtained from the difference between the fitted branching ratios at the minimum $\chi^2 = \chi^2_{\mathrm{min}}$ and at $\chi^2_{\mathrm{min}} \pm 1$. To account for the relatively large χ^2, the systematic error was deduced from the fit corresponding to $\chi^2_{\mathrm{min}} \pm 1.47$. The TAC-ADC nonlinearity correction reduced the χ^2 by 20%, but changed the branching ratio by only 0.03% when the same fitting region was used. Minor distortions in the timing spectra due to TAC-ADC nonlinearities, which were not fully eliminated by the rebinning mentioned above, were responsible for the major part of the observed χ^2. The nonlinearities caused a small dependence of R' on the fitting region consistent with the systematic error indicated. Because the uncertainty of the fit was already included in the systematic uncertainty of the branching ratio when the large χ^2 effect was taken into account, no additional uncertainty from this effect was added.

A component with a time dependence $\int_t^{t+\Delta} \theta(t') f(t') dt'$ was added to the above equation to simulate the effect of the detection inefficiency for charged-particle pileup into TINA around the time of the event due to finite pulse width; a typical value was $\Delta = 40$ ns for the inefficient time period. This component is characterized by an increase of the background level with time in the region ~30 ns before t_0 in the time spectrum for the high-energy region ($\pi \to e\nu$). Tight beam prepileup cuts (see Sec. III B) were developed to reduce the effect to a negligible level and this component was omitted in the final fit.

Other potential systematic effects were studied in the fitting procedure by introducing a term to account for possible distortion caused by the rate dependence of the pileup rejection, and by freeing fitting parameters such as the pion decay rate, the muon decay rate, and the timing resolution. Typically, these effects were at the 0.05% level and were omitted.

IV. CORRECTIONS

Various corrections to the raw branching ratio, including the largest correction for the low-energy tail of $\pi \to e\nu$ decay events, were obtained empirically. Monte Carlo (MC) calculations were used to simulate systematic effects related to positron annihilation in flight, scattering of positrons leading to pathological triggers, false vetoes, and loss of low-energy positrons. The MC calculations were also used to verify the effect of applying cuts on the acceptance using the wire chambers.

A. Monte Carlo corrections

The processes included in the MC calculations were energy loss due to ionization and bremsstrahlung, positron annihilation in flight or at rest, and subsequent γ-ray emission, multiple Coulomb scattering, Bhabha scattering, and Møller scattering. Pions were generated according to the measured stopping distribution in the target. For $\pi \to e\nu$ a pion decayed isotropically to a positron which was traced until it stopped or escaped from the detector system; the radiative decay of the pion $\pi \to e\nu\gamma$ was not included in this part of the MC calculation but separately folded into the response function of TINA. For $\pi \to \mu \to e$, muons were distributed randomly on a sphere of radius 1.5 mm (corresponding to the range of 4-MeV muons) from the original pion location and then decayed isotropically to positrons. The effect of muon polarization, estimated to be at the level of 0.02% on R_{expt}, was neglected. The process $\pi \to \mu\nu\gamma$ was also neglected in the MC calculations but $\mu \to e\nu\bar{\nu}\gamma$ was included. The detection efficiency of photons from the radiative muon decay was assumed to be 100% if they were emitted toward TINA. When Bhabha (or Møller) scattering occurred in the path of a positron (electron), a new electron was generated according to the kinematics. Because the target was thick compared to a mean free path for Bhabha scattering with a low-energy secondary electron, each path was divided into 5-mm steps—a smaller step size made no difference in the result. Energy loss, multiple scattering, Bhabha scattering, and annihilation were calculated for each step.

The effects of Bhabha scattering were reproduced well by the Monte Carlo program. In the experimental data, 2.5–4 % of events (depending on the diameter of the wire-chamber cut) were multitrack events and the corresponding prediction from Monte Carlo calculation agreed for each diameter of wire-chamber cut within 10% of the effect. The uncertainty arising from the hit position of the wire chambers was of the same order.

There was a strong dependence of the measured branching ratio on the diameter of the wire-chamber cut

as shown by the solid circles in Fig. 7. The branching ratio without the wire-chamber fiducial cut was smaller by 0.5% than that with a cut at the diameter corresponding to the profile of the trigger counter $T4$ (the standard cut). Some fraction of the dependence (0.1% at large diameter cuts and significantly higher at a small diameter) was attributed to the change in the low-energy fraction of the $\pi \to e\nu$ peak; i.e., requiring only the center region of TINA for positron detection affected the response function by reducing the low-energy tail. The remainder of the dependence (0.3–0.4 %) was due to multiple Coulomb scattering in the scintillators and the wire-chamber frames. As shown by the open circles in Fig. 7, the dependence was removed after the corrections were applied to compensate for these effects.

The fraction of events hitting the $V0$ counter, in addition to firing all the trigger counters, was ~0.6%. These were rejected in the analysis in order to minimize events which originated from old muon decays in the $V0$ counter. In the MC calculations, however, 0.15% were attributed to Bhabha scattering in the target and 0.15% to backscattering from the wire chamber frames, leaving ~0.3% for the contribution from old muons in $V0$. The effect of rejecting these events on the branching ratio was estimated from the MC calculation to be 0.08%, in agreement with the 0.12 ± 0.05 % change when these events were included in the analysis.

The beam pileup detection logic on the $B1$, VL, and VR counters falsely rejected some events if these counters fired due to Bhabha scattering. The MC calculation was used to estimate the effect on the branching ratio to be of the order of 0.1%. Because the thresholds of the LR and LL counters were around 1 MeV (the expected positron energy loss is ~0.3 MeV) and the fraction of positron events leaving energy above the threshold in these counters was only 0.01%, the vetoing effect of the counters VL and VR was neglected in the MC calculation.

The fraction of low-energy $\pi \to \mu \to e$ positrons stopping in the target or T counters before causing a trigger was of the order of 0.2%. The agreement in the size of the two low-energy peaks in Fig. 2 (0.7% of the total events for both MC and data) confirmed the validity of the MC calculations in the low-energy region. The effects of the radiative muon decay $\mu \to e\nu\bar{\nu}\gamma$ were small (~0.02%).

The multiplicative correction to R' obtained from the MC calculations for the above-mentioned effects was 1.0027 ± 0.0011. The estimated systematic error included the uncertainties in the positions and thicknesses of the counters ($\leq$0.03%), and the beam stopping distribution in the target (0.05%). The uncertainty for the step size effect (0.03%) was estimated from the difference between 5-mm and 2.5-mm calculations. All uncertainties were added in quadrature.

B. Tail correction

The largest potential source of systematic uncertainty in the measurement of the branching ratio arose from the low-energy tail of the $\pi \to e\nu$ peak which extended under the $\pi \to \mu \to e$ distribution. The tail was due mostly to the response function of TINA; the component due to radiative processes was small (about 0.4%) because NaI is also sensitive to the forward-peaked bremsstrahlung γ rays emitted in the $\pi \to e\nu\gamma$ decay.

The response functions of TINA, measured in the direct positron beam at different incident angles, were summed with weights according to the solid angle of acceptance for $\pi \to e\nu$ events. The result was convoluted with the radiative line shape obtained from the MC calculation. However, because of apparent low-energy components in the positron beam due to slit scattering and beam momentum dispersion, the line shape measured by this method could give only an upper limit of the low-energy tail of $\pi \to e\nu$ events.

In order to estimate the $\pi \to e\nu$ tail correction, it was necessary to suppress the dominant $\pi \to \mu \to e$ component. This was done by applying two techniques [27]. First, by exploiting the short pion lifetime (26 ns) compared to the muon lifetime (2 μs), positrons accepted in the first 30 ns after the pion stop were enriched in $\pi \to e\nu$ events by a factor of ~100. The second technique used energy-loss and pulse-shape information from the $B3$ stopping counter. For $\pi \to e\nu$ decay, the energy loss in $B3$ included the kinetic energy of the stopping pion plus a small contribution from the exiting decay positron. For events from the $\pi \to \mu \to e$ chain, there was an additional 4-MeV component from the kinetic energy of the decay muon which stopped within the $B3$ counter. (A very small fraction of these muons penetrated into the $B4$ counter which was also inspected for additional energy.) As shown in Fig. 8, there are two peaks in the spectrum of total energy deposited in the $B3$ target counter (the horizontal axis) corresponding to the two processes. The cut positions shown by the vertical lines in Fig. 8 provided a factor of 100 suppression of the background. The presence of a muon in an event was also identified by comparing the integrated charge from $B3$ and the early part of the charge measured in several ADC's; one with a narrow and early time gate was sensitive mainly to the stopping pion component. Cuts

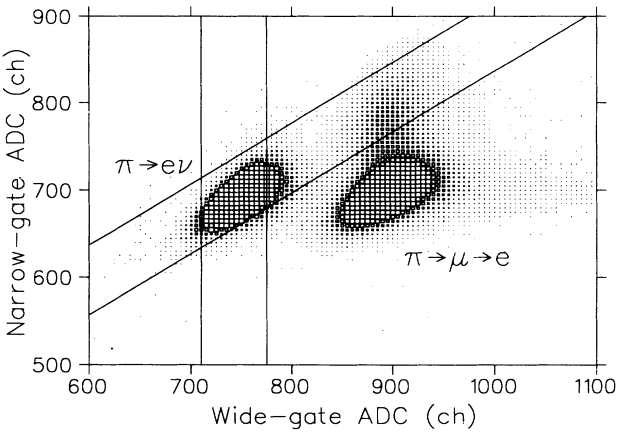

FIG. 8. Total target energy observed with the wide-gate ADC vs the early part of the pulse observed with the narrow-gate ADC for $\pi \to e\nu$ events (the low-energy peak) and $\pi \to \mu \to e$ events (the high-energy peak). The density scale is nonlinear and the $\pi \to e\nu$ events are enhanced by 100 times for this figure. The lines show the cuts to select $\pi \to e\nu$ events.

on the two-dimensional distribution of wide-gate versus narrow-gate ADC counts (see diagonal lines in Fig. 8) were applied for an additional suppression of $\pi \to \mu \to e$ events. The cuts were optimized to maximize the ratio $N_{\text{peak}}/\sqrt{N_{\text{tail}}}$, where N_{peak} and N_{tail} are the number of events above and below the threshold at channel 3400 in TINA's energy spectrum, respectively. The background-suppressed spectrum in Fig. 9 shows a total suppression factor of 10^5 for the $\pi \to \mu \to e$ background, while retaining 73% of $\pi \to e\nu$ events in the early 30-ns time window. The time spectrum and target-energy distribution of the residual $\pi \to \mu \to e$ background indicated that the origin of these events was mostly from pion decays in flight in which a muon stopped in the target, depositing a similar energy to that of a beam pion.

In order to extract the low-energy fraction of $\pi^+ \to e^+\nu$ events, the procedure to fit the background-suppressed spectrum required knowledge of the shape of the tail, as well as the $\mu^+ \to e^+\nu\bar{\nu}$ background. The latter was obtained from late-decay events in the time region $t > 150$ ns. Several different functions for the tail, such as a linear or exponential tail, gave an average tail fraction of 1.5±0.3%. Reasonable justification could not be given for any particular line shape, and the fitting method was only used as a consistency check of the following analysis.

To constrain the absolute value of the tail, a procedure was developed to establish lower and upper limits on the tail fraction from the background-suppressed $\pi \to e\nu$ spectrum. An unambiguous lower limit on the tail was found as follows: The counts in the suppressed spectrum were summed from zero to an arbitrary energy E_a ($E_a \leq 52.3$ MeV), giving a total of N_a counts. Assuming all these events were $\pi \to \mu \to e$ positrons, the total number of such events from 0 to 52.3 MeV was calculated using the measured $\mu^+ \to e^+\nu\bar{\nu}$ distribution. Subtracting this number from the total counts in the suppressed spectrum below 52.3 MeV yielded a lower limit on the $\pi \to e\nu$ tail. This procedure was repeated for $0 \leq E_a \leq 52.3$. For small values of E_a, the assumption of no tail counts in the energy region ($0 \leq E \leq E_a$) was relatively good, but the statistical significance of N_a was poor. As E_a was increased the assumption becomes worse, but the statistics better. A lower limit on the tail as a function of E_a is shown by the solid circles in Fig. 10.

To establish an upper limit, the independently measured response function in TINA, convoluted with the radiative tail, was used to modify the above procedure. For each cutoff E_a, this response function was summed from 0 to E_a and the number of counts subtracted from N_a before the extrapolation to 52.3 MeV was performed. In this way, too many events were assumed to be genuine tail events, because the response function measured in the direct beam was known to contain additional low-energy components. An upper limit on the tail fraction was thus established as shown by the open circles in Fig. 10. If the response function had been correct, then this upper limit curve should be constant as E_a was varied and should represent the actual value of the tail.

It can be seen that the upper and lower limits in Fig. 10 constrain the same value from above and below. An average of the two points with the tightest constraints (including 1σ errors) as indicated by the arrows in Fig. 10 was used as an estimate of the actual value of the tail (1.44%) in the suppressed data spectrum. Half the difference between these two constraints was taken as the error estimate (±0.24%).

The suppression technique required several other factors to be taken into account. In eliminating events with an extra 4-MeV muon in $B3$, there was a bias against positrons with large energy deposition in the same counter. This effect led to a 170 ± 35-keV shift in the energy scale of the suppressed spectrum with respect to the unsuppressed spectrum, resulting in a 0.05% difference in the tail fraction between the two. This shift was taken into account in the evaluation of the tail using the background-suppressed data as mentioned above, as well as in subtracting the $\pi \to \mu \to e$ background spectrum.

Other effects that could distort the tail of the NaI response function were evaluated using Monte Carlo calculations. The major potential source of distortion arose from Bhabha scattering within $B3$, where the e^- was

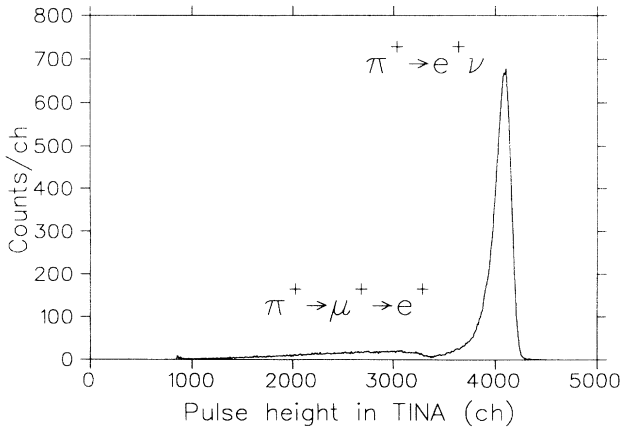

FIG. 9. Positron spectrum after suppression techniques described in the text.

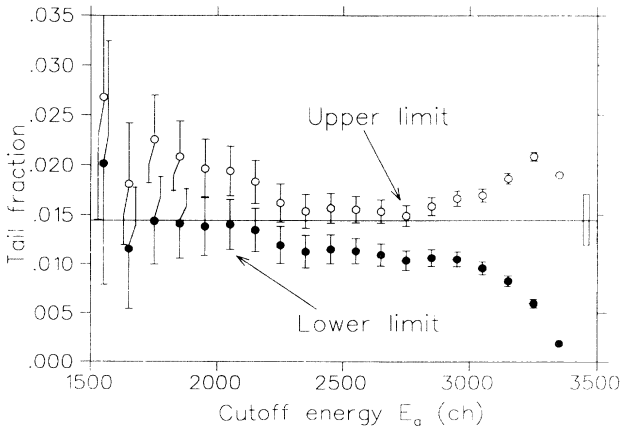

FIG. 10. Lower (solid circles) and upper (open circles) limits of the fraction of the low-energy tail. The horizontal line indicates the value of the raw tail correction derived from the two points labeled by the arrows as described in the text, and the vertical bar at the right indicates the error assigned.

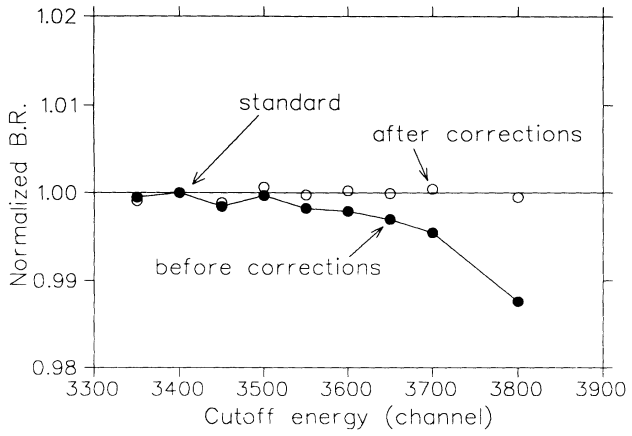

FIG. 11. Effects of cutoff energy. The branching ratios are normalized to the standard value at channel 3400. The solid circles indicate values without the Monte Carlo and energy-shift corrections. The open circles indicate values with full corrections.

responsible for the trigger, while the e^+ passed through the wire-chamber frames losing energy and contributing to the tail. This process was most probable for events with long path lengths in $B3$ and tended to leave more energy in $B3$ due to additional energy loss produced by the presence of two exiting particles. Such events were therefore preferentially rejected. Monte Carlo calculations indicated that 0.44% of $\pi \to e\nu$ events fell into the region with the positron energy $E < 56.4$ MeV (corresponding to the standard cutoff at 3400 ch) and positron energy loss in $B3$, $\Delta E_{B3} > 2.2$ MeV (corresponding to the threshold for positron energy loss). This additional correction factor was insensitive to the variation of the cutoff energy of TINA or the threshold of the $B3$ counter; a 1-MeV shift in TINA's energy calibration only changed the correction by 0.02%. The correction factor varied only by 0.02% with a $B3$ threshold change from 2.2 MeV to 1.4 MeV.

Combining all the above factors, the overall multiplicative tail correction obtained was 1.0193 ± 0.0025. The validity of the tail correction was tested by observing that the branching ratio result after the tail correction was applied was insensitive within 0.1% to the lower cutoff energy chosen for defining the $\pi \to e\nu$ peak in the range from 54.5 MeV (near the edge of the $\mu^+ \to e^+\nu\bar{\nu}$ decay) to 64.5 MeV (~8% tail correction). This dependence is shown in Fig. 11, where the solid circles indicate the results without corrections for the biasing effects and the open circles, with full corrections.

C. Other corrections

Good events might have been falsely rejected because of spurious hits in the vetoing counters. The effects of Bhabha and large-angle scattering have already been described in the MC studies except for the effect of the $V1$ counter. The possible sources of false veto in $V1$ were primarily backscattering or electromagnetic shower leakage from TINA because of its proximity to the crystal. This effect was studied by looking at samples of the events with a hit in the $V1$ counter. A multiplicative correction factor was estimated to be 1.0009 ± 0.0005. To avoid a possible backscattering effect, the wire-chamber cut did not remove multitrack events, although the amount of backscattering was empirically estimated to be at most $0.1 \pm 0.1\%$. Backscattering and leakage of electromagnetic showers from TINA to the T counters would also cause event rejection by the energy-loss cut whose bias was estimated to be negligible (see Sec. III B). Because the other counters were much smaller and farther from TINA than the wire chambers and the T counters, further effects were neglected.

Because wire chambers were required as a part of the event definition logic in the off-line analysis, possible energy-dependent effects due, for example, to energy-loss variations were studied. A sample of events having only one track near the center of one of the chambers was used to determine the efficiency of the other chamber as a function of positron energy. Inefficiencies of the wire chambers were observed to be $< 2\%$ during the run. No energy-dependent effect was found and the net multiplicative correction was 0.9998 ± 0.0004. No efficiency loss correction was necessary for the T counters.

The timing of the event was based on the signal from energy loss in the $T4$ counter and was expected to be insensitive to the positron energy. Nevertheless, a time zero shift between the low- and high-energy timing spectra could have biased the branching ratio measurement and was estimated using muon decay time spectra. Positive muons stopping at the same depth as the pions in the target provided time spectra with a "step function" at time zero which were fitted to an error function. The measured time zero for different positron energy regions indicated no significant energy dependence except for the low-energy region (0.2 ± 0.1 ns shift below 12 MeV). Taking the weighted average of the time zero shifts, the multiplicative correction was estimated 0.9998 ± 0.0008.

The calibration of the TAC-ADC spectrum, 53.335 ± 0.020 ps/channel, implied an uncertainty in the branching ratio $1.0000 \pm 0.000\,28$, which was estimated by fitting timing spectra for different calibration constants. The error in the pion lifetime [22] contributed an additional uncertainty of 1.0000 ± 0.0009.

V. RESULTS

The corrections applied to the raw branching ratio are summarized in Table I where all systematic uncertainties are combined in quadrature. The result [24] is

$$R_{\text{expt}} = 1.2265 \pm 0.0034(\text{stat}) \pm 0.0044(\text{sys}) \times 10^{-4}. \quad (4)$$

The result is in good agreement with the standard model expectation R_{th} [Eq. (1)] and the previous measurement [23] as well as with the recent measurement by Czapek *et al.* [25], $R_{\text{expt}} = 1.2346 \pm 0.0035(\text{stat}) \pm 0.0036(\text{sys}) \times 10^{-4}$ (for discussions using combined results, see Ref. [28]).

VI. DISCUSSION

A quantitative comparison with the standard model prediction can be obtained by writing $R_{\text{expt}} =$

TABLE I. $\pi \to e\nu$ branching ratio summary.

Raw branching ratio R' ($\times 10^{-4}$)	1.1994 ± 0.0034(stat) ± 0.0023(sys)
Multiplicative corrections	
Tail correction	1.0193 ± 0.0025
Pion stop time t_0	0.9998 ± 0.0008
Time calibration	1.0000 ± 0.0003
Monte Carlo	1.0027 ± 0.0011
$V1$ veto	1.0009 ± 0.0005
Wire-chamber inefficiency	0.9998 ± 0.0004
π lifetime	1.0000 ± 0.0009
Branching ratio $R_{\rm expt}$ ($\times 10^{-4}$)	1.2265 ± 0.0034(stat) ± 0.0044(sys)

$(g_e/g_\mu)^2 R_{\rm th}$, where g_e and g_μ are the electroweak couplings of the electron and muon, respectively. The result is $g_e/g_\mu = 0.9966 \pm 0.0023$ where unity corresponds to perfect e-μ universality. Lepton universality in the charged-current mode is also tested with τ and W leptonic decays. Table II summarizes the present status of e-μ universality tests. The relative branching ratios of the decays of the W boson to charged leptons and associated neutrinos give a straightforward test of lepton universality for the three generations. However, because of low statistics the precision has been limited to the level of 4–7 % [29]. Comparison of the world-average branching ratios of τ decays [22, 30], $B(\tau \to e\nu\overline{\nu}) = 0.1794 \pm 0.0027$ and $B(\tau \to \mu\nu\overline{\nu}) = 0.1733 \pm 0.0029$, with a phase space correction of 0.9728 ± 0.0001 provided the ratio of the coupling constants $g_e/g_\mu = 1.004 \pm 0.011$. Inverse reactions using ν_e and ν_μ beams also gave a ratio of the coupling constants $g_e/g_\mu = 1.10 \pm 0.05$ [31]. As shown in Table II, all the data are consistent with universality and the branching ratio of the decays $\pi^+ \to e^+\nu$ and $\pi^+ \to \mu^+\nu$ provides the most stringent constraint.

For universality extended to the three generations, measurements of the τ decay rate [22] and $W \to l\nu$ ($l = e, \mu, \tau$) decays [29] test $\tau - \mu$ and $\tau - e$ universality at the 3% and 7% levels, respectively. The ratio g_τ/g_e can also be deduced [32] using the branching ratios of the decays $\tau \to \pi\nu_\tau$ and $\pi^+ \to e^+\nu$, to give $g_\tau/g_e = 0.985 \pm 0.026$.

Alternatively, if universality is assumed, the present result can be used to obtain a limit on a hypothetical pseudoscalar coupling $f_p = (-0.0034 \pm 0.0023) f_\pi m_e$, where f_π is the pion decay constant and m_e is the electron mass. Following the same procedure as Ref. [33] using the present result at 90% C.L., an upper limit for the tensor coupling constant relative to the ordinary weak coupling was also obtained to be $\mid f_T \mid \leq 10^{-4}$. The experimental ratio of the coupling constants can be used to constrain some models. Based on Shanker's phenomenological analyses [11] with an assumption that the contributions from hypothetical processes add up constructively, a mass bound on a vector leptoquark is obtained to be $m_{vq} \geq 200$ TeV/c^2. The mass bound for the pseudoscalar leptoquark is 1.3 TeV/c^2. Similarly, a mass bound on a charged Higgs particle, which couples to the leptons like the W boson, is obtained to be $m_H \geq 2$ TeV/c^2. The masses ($m_{\rm SS}$) of the particles with pseudoscalar interactions arising in the supersymmetric models can be also constrained to be $m_{\rm SS} > 0.6$ TeV/c^2 for the case when all the masses are degenerate, and $m_{\rm SS} > 2$ TeV/c^2 for the case when one of the particles has a large mass.

TABLE II. Summary of e-μ universality tests.

Process	g_e/g_μ	Ref.
π decay	0.9966±0.0023	This work
τ decay	1.004±0.011	[22, 32]
ν_e, ν_μ scattering	1.10±0.05	[31]
W decay	0.99±0.04	[29]

In the presence of the Majoron M (a Nambu-Goldstone boson arising in a gauge model with spontaneous breaking of the global $B - L$ symmetry) [9], the expected $\pi \to e\nu$ branching ratio is slightly higher:

$$\frac{\Gamma(\pi \to eL^0)/\Gamma(\pi \to \mu L^0)}{\Gamma(\pi \to e\nu)/\Gamma(\pi \to \mu\nu)} = 1 + 157.5 g_M^2, \qquad (5)$$

where L^0 includes the final states ν, νM, and $\nu\chi$ (χ is a very light Higgs particle). Using the upper limit of the measured branching ratio, one can obtain the limit on the Majoron-neutrino coupling constant $g_M^2 < 3 \times 10^{-5}$ (90% C.L.).

The measured branching ratio is also sensitive to the presence of massive neutrinos [5]. Limits on the neutrino mixing parameter $\mid U_{ei} \mid^2$ between the weak electron-neutrino eigenstate and the mass eigenstate m_{ν_i} have been deduced and discussed for the case of $m_\nu \leq m_\pi$ in Ref. [34]. In the region $m_\nu \geq m_\pi$—for a fourth-generation neutrino, the region $m_\nu \geq m_{Z^0}/2$ is still open—the strength of the process is absorbed by the massive fourth-generation neutrino through mixing, and the experimental branching ratio is expressed as $\frac{R_{\rm expt}}{R_{\rm th}} = \frac{1-|U_{e4}|^2}{1-|U_{\mu 4}|^2}$. An upper bound (90% C.L.) on the deviation from the theoretical prediction was obtained, $R_{\rm expt}/R_{\rm th} \leq 1.0045$. With an assumption $\mid U_{e4} \mid << \mid U_{\mu 4} \mid$, the limit of the ratio of the experimental and expected branching ratios implies $\mid U_{\mu 4} \mid^2 \leq 0.0045$.

ACKNOWLEDGMENTS

We are pleased to acknowledge the assistance of B. H. Olaniyi and J. Summhammer, and the technical help of C. Lim, C. Stevens, and S. Chan. We also thank D. F. Measday for the use of TINA. This work was supported by the Natural Sciences and Engineering Research Council and the National Research Council of Canada.

[1] T. Fazzini *et al.*, Phys. Rev. Lett. **1**, 247 (1958); G. Impeduglia *et al.*, *ibid.* **1**, 249 (1958).
[2] M. Ruderman and R. Finkelstein, Phys. Rev. **76**, 1458 (1949); E.C.G. Sudarshan and R.E. Marshak, *ibid.* **109**, 1860 (1958); R.P. Feynman and M. Gell-Mann, *ibid.* **109**, 193 (1958).
[3] W.J. Marciano, in *Proceedings of the Workshop on Future Directions in Nuclear and Particle Physics at Multi-GeV Hadron Beam Facilities*, Upton, New York, 1993, edited by D. F. Geesaman (Brookhaven National Laboratory Report No. BNL-52389, Upton, NY, 1993), p. 82.
[4] W.J. Marciano, Phys. Rev. D **45**, R721 (1992); M. Fukugita *et al.*, Phys. Lett. B **283**, 142 (1992).
[5] J.N. Ng, Nucl. Phys. **B191**, 125 (1981); R.E. Shrock, Phys. Rev. D **24**, 1232 (1981).
[6] K. Enqvist, K. Mursula, and M. Roos, Z. Phys. C **21**, 133 (1983).
[7] X. Li and E. Ma, Phys. Rev. Lett. **47**, 1788 (1981).
[8] Fayyazuddin and Riazuddin, Phys. Rev. D **35**, 2201 (1987).
[9] G.B. Gelmini and M. Roncadelli, Phys. Lett. **99B**, 411 (1981); see also C.E. Picciotto *et al.*, Phys. Rev. D **37**, 1131 (1988); V. Barger, W.Y. Keung, and S. Pakvasa, *ibid.* **25**, 907 (1982).
[10] J.F. Donoghue and L.F. Li, Phys. Rev. D **19**, 945 (1979); B. McWilliams and L.F. Li, Nucl. Phys. **B179**, 62 (1981); H.E. Haber, G.L. Kane, and T. Sterling, *ibid.* **B161**, 493 (1979).
[11] O. Shanker, Nucl. Phys. **B204**, 375 (1982).
[12] S.M. Berman, Phys. Rev. Lett. **1**, 468 (1958).
[13] T. Kinoshita, Phys. Rev. Lett. **2**, 477 (1959).
[14] T. Goldman and W.J. Wilson, Phys. Rev. D **14**, 2428 (1976).
[15] W.J. Marciano and A. Sirlin, Phys. Rev. Lett. **36**, 1425 (1976).
[16] T. Goldman and W.J. Wilson, Phys. Rev. D **15**, 709 (1977).
[17] V.N. Bolotov *et al.*, Phys. Lett. B **243**, 308 (1990); L.E. Piilonen *et al.*, Phys. Rev. Lett. **57**, 1402 (1986).
[18] S. Egli *et al.*, Phys. Lett. B **222**, 533 (1989).
[19] M.V. Terent'ev, Yad. Fiz. **16**, 809 (1972) [Sov. J. Nucl. Phys. **16**, 449 (1973)].
[20] H.L. Anderson *et al.*, Phys. Rev. **119**, 2050 (1960).
[21] E. Di Capua *et al.*, Phys. Rev. **133**, B1333 (1964).
[22] Particle Data Group, K. Hikasa *et al.*, Phys. Rev. D **45**, S1 (1992).
[23] D.A. Bryman *et al.*, Phys. Rev. D **33**, 1211 (1986).
[24] D.I. Britton *et al.*, Phys. Rev. Lett. **68**, 3000 (1992).
[25] G. Czapek *et al.*, Phys. Rev. Lett. **70**, 17 (1993).
[26] F. James and M. Roos, Computer code MINUIT, CERN Report No. DD/75/20, 1975 (unpublished).
[27] G. Azuelos *et al.*, Phys. Rev. Lett. **56**, 2241 (1986).
[28] T. Numao, Mod. Phys. Lett. A **36**, 3357 (1992); D.A. Bryman, Comments Nucl. Part. Phys. **21**, 101 (1993).
[29] F. Abe *et al.*, Phys. Rev. Lett. **68**, 3399 (1992); F. Abe *et al.*, *ibid.* **69**, 28 (1992); J. Alitti *et al.*, Z. Phys. C **52**, 209 (1991).
[30] W.J. Marciano and A. Sirlin, Phys. Rev. Lett. **61**, 1815 (1988).
[31] J.V. Allaby *et al.*, Phys. Lett. B **179**, 301 (1986).
[32] D.A. Bryman, Phys. Rev. D **46**, 1064 (1992).
[33] M.B. Voloshin, Phys. Lett. B **283**, 120 (1992).
[34] D.I. Britton *et al.*, Phys. Rev. D **46**, R885 (1992).

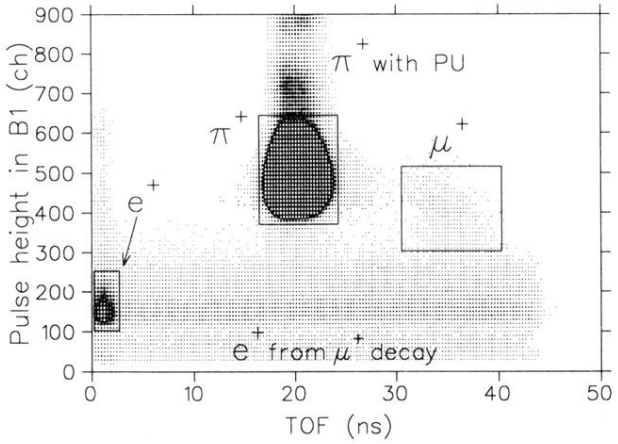

FIG. 4. TOF vs pulse heights in the $B1$ counter. Boxes indicate beam particles. Some counts above the boxes are due to an additional particle in the same ADC gate (indicated by PU). The density scale is nonlinear in order to enhance rare events.

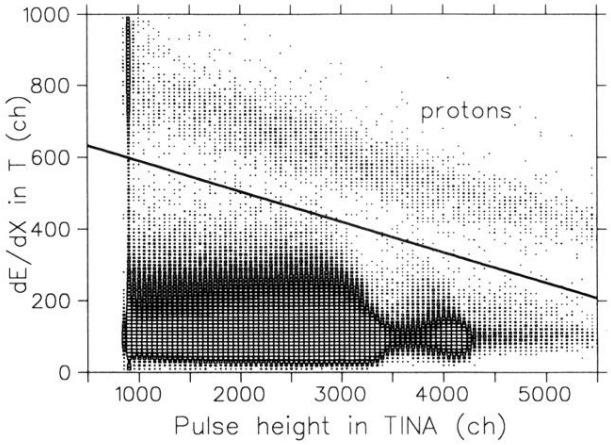

FIG. 5. TINA energy vs energy loss in the T counters. The heavy line indicates the cut position used to eliminate protons. The density scale is nonlinear.

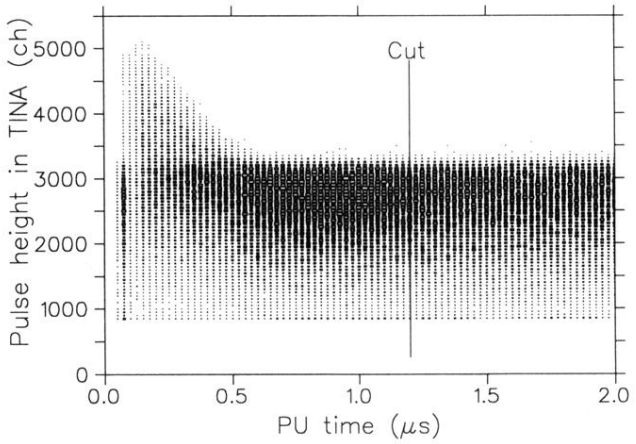

FIG. 6. Time of postpileup vs TINA energy. The vertical line indicates the cutoff time at 1.2 μs which rejected $\sim$3% of good events.

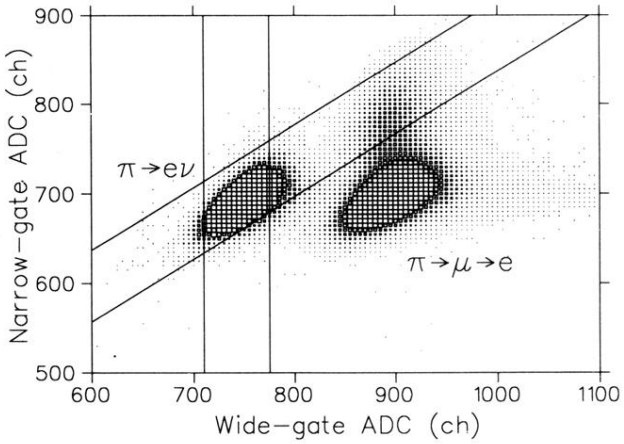

FIG. 8. Total target energy observed with the wide-gate ADC vs the early part of the pulse observed with the narrow-gate ADC for $\pi \rightarrow e\nu$ events (the low-energy peak) and $\pi \rightarrow \mu \rightarrow e$ events (the high-energy peak). The density scale is nonlinear and the $\pi \rightarrow e\nu$ events are enhanced by 100 times for this figure. The lines show the cuts to select $\pi \rightarrow e\nu$ events.